Hysteresis drives cell-cycle transitions in *Xenopus laevis* egg extracts

Wei Sha*, Jonathan Moore†, Katherine Chen*, Antonio D. Lassaletta*, Chung-Seon Yi*, John J. Tyson*, and Jill C. Sible*‡

*Department of Biology, Virginia Polytechnic Institute and State University, Blacksburg, VA 24061-0406; and †Cancer Research UK London Research Institute, Clare Hall Labs, South Mimms, Herts, EN6 3LD, United Kingdom

Edited by Thomas D. Pollard, Yale University, New Haven, CT, and approved November 21, 2002 (received for review September 3, 2002)

Cells progressing through the cell cycle must commit irreversibly to mitosis without slipping back to interphase before properly segregating their chromosomes. A mathematical model of cell-cycle progression in cell-free egg extracts from frog predicts that irreversible transitions into and out of mitosis are driven by hysteresis in the molecular control system. Hysteresis refers to toggle-like switching behavior in a dynamical system. In the mathematical model, the toggle switch is created by positive feedback in the phosphorylation reactions controlling the activity of Cdc2, a protein kinase bound to its regulatory subunit, cyclin B. To determine whether hysteresis underlies entry into and exit from mitosis in cell-free egg extracts, we tested three predictions of the Novak–Tyson model. (*i*) The minimal concentration of cyclin B necessary to drive an interphase extract into mitosis is distinctly higher than the minimal concentration necessary to hold a mitotic extract in mitosis, evidence for hysteresis. (*ii*) Unreplicated DNA elevates the cyclin threshold for Cdc2 activation, indication that checkpoints operate by enlarging the hysteresis loop. (*iii*) A dramatic "slowing down" in the rate of Cdc2 activation is detected at concentrations of cyclin B marginally above the activation threshold. All three predictions were validated. These observations confirm hysteresis as the driving force for cell-cycle transitions into and out of mitosis.

The biochemical oscillations that characterize early cell cycles of South African clawed frog, *Xenopus laevis*, can be reconstituted in cell-free egg extracts (1, 2). In this system, newly synthesized cyclin B associates with the cyclin-dependent kinase (Cdk) Cdc2 (3, 4). (Cyclin B/Cdc2 dimers are referred to as M-phase promoting factor.) Cyclin B/Cdc2 is rapidly inhibited by phosphorylation of Cdc2 on tyrosine 15 by two kinases, Wee1 and Myt1 (5, 6). Cdc2 remains inactive until this phosphate group is removed by the phosphatase, Cdc25 (7, 8). In turn, active Cdc2 phosphorylates and inhibits Wee1 (9) and phosphorylates and activates Cdc25 (10, 11). These positive feedback loops are responsible for the abrupt activation of cyclin B/Cdc2 at the G_2/M transition. Also important to this control system is a negative feedback loop in which active Cdc2 indirectly activates Fizzy, a protein that targets cyclin B for degradation via the ubiquitin–proteasome pathway (12, 13). Entry into mitosis is triggered by synthesis of cyclin B (1, 4), and exit from mitosis is triggered by degradation of cyclin B (14–16).

The cell cycle of frog egg extracts was selected as the first case for building a comprehensive mathematical model of the cell-cycle engine (17) because egg extracts contain the simplest functional control system for activation of the Cdks that drive cell-cycle transitions. The Novak–Tyson equations model this network of interlocking positive and negative feedback loops. In the model, the positive feedback loops create alternative states of low and high Cdc2 activity (interphase and M phase, respectively), and the negative feedback loop drives the control system back and forth between these states (Fig. 1*a*). During interphase, Cdc2 activity is low (because Cdc2 is phosphorylated), the rate of cyclin synthesis exceeds the rate of cyclin degradation, and cyclin accumulates in the extract. When total cyclin concentration exceeds an activation threshold (Fig. 1*a*), Cdc2 is abruptly activated by removal of the inhibitory phosphate groups. Because Cdc2 activates cyclin proteolysis, the rate of cyclin degradation in M phase exceeds its rate of synthesis, and cyclin concentration falls. However, according to the model, the extract stays in the "activated state" (unphosphorylated Cdc2 and rapid cyclin degradation) until Cdc2 activity falls below an inactivation threshold (Fig. 1*a*), when Cdc2 is abruptly inactivated by tyrosine phosphorylation. This cycle of events is called a hysteresis loop. Hysteresis underlies behaviors like ferromagnetism and DNA melting/reannealing. In both cases, the value of a control parameter (magnetic field, temperature) that induces a transition from one state to another is quite different from the value needed to induce the reverse transition.

Hysteretic transitions are discontinuous. Once the system has been switched on by moving the control parameter across the activation threshold, it cannot be switched off by bringing the control parameter back across the activation threshold in the opposite direction. Nonhysteretic switches behave differently, switching on and off at the same value. A reversible Cdc2 switch would look like Fig. 1*b*.

Although several authors have suggested that progress through the cell cycle is governed by a hysteresis loop like Fig. 1*a* (17, 20–23), there is another theoretically plausible explanation for switch-like behavior at mitosis. Periodic cyclin degradation could be driven by a time-delayed negative feedback loop involving Cdc2 activation of Fizzy, without participation from Wee1 and Cdc25. Such a model was proposed by Goldbeter (19) and is consistent with a nonhysteretic switch (Fig. 1*b*). The distinction between these two pictures had not been investigated experimentally until now.

Cyclin thresholds for entry into or exit from mitosis have been measured experimentally. Solomon *et al.* (4) demonstrated that there is a cyclin threshold for Cdc2 activation at mitosis 1 in frog egg extracts. Subsequently, Holloway *et al.* (15) and Stemmann *et al.* (16) demonstrated a cyclin threshold for exit from mitosis. All of these experiments are consistent with either Fig. 1 *a* or *b*. In this study, we measure the thresholds for Cdc2 activation and inactivation going into and out of the same mitosis to distinguish between the mechanisms proposed in Fig. 1*a* (hysteretic) and Fig. 1*b* (nonhysteretic).

Another distinction between Fig. 1 *a* and *b* is that, in the case of hysteresis, the underlying dynamical system is bistable. That is, for certain fixed values of the control parameter, the governing dynamical equations admit two different stable steady-state solutions separated by an unstable steady state (Fig. 1*a*). (Stable and unstable steady states are illustrated by a ball rolling on an undulating landscape. At the bottom of any pit ∪, the ball is in a stable steady state, whereas, if balanced at the top of a hill ∩,

This paper was submitted directly (Track II) to the PNAS office.

Abbreviations: Cdk, cyclin-dependent kinase; Δcyclin B, recombinant, nondegradable human cyclin B; CSF, cytostatic factor; CHX, cycloheximide; APH, aphidicolin.

See commentary on page 771.

‡To whom correspondence should be addressed. E-mail: siblej@vt.edu.

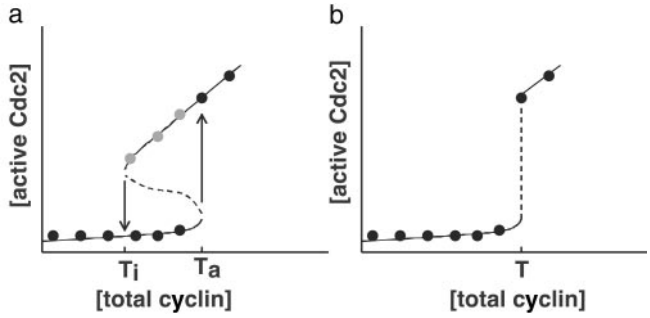

Fig. 1. Steady-state activity of Cdc2 in a frog egg extract plotted as a function of total concentration of cyclin. A threshold concentration of cyclin for activation of Cdc2 was demonstrated by Solomon *et al.* (4). These data are schematically represented by the black circles. (*a*) Theoretical prediction of bistability and hysteresis in the Cdc2 control system (17, 18). An S-shaped curve is delineated by two thresholds, T_i and T_a. For a fixed concentration of cyclin between T_i and T_a, the control system has two stable steady states (black and gray circles), corresponding to interphase (low Cdc2 activity) and mitosis (high Cdc2 activity), separated by an unstable steady state (intermediate Cdc2 activity along the dashed line). If cyclin concentration is elevated above its activation threshold the extract will transit irreversibly from interphase into mitosis (↑). To make the reverse transition from mitosis back to interphase (↓), cyclin concentration must drop below the inactivation threshold. The stable steady states represented by gray circles have not previously been observed experimentally. (*b*) In an alternative account of the data by Goldbeter (19), the activation threshold and inactivation threshold concentrations of cyclin are identical. Both models are consistent with the measurements of Solomon *et al.* (4).

the ball is in an unstable steady state.) Bistability underlies the decision of an oocyte to initiate maturation, by activation of the mitogen-activated protein kinase signaling cascade (24) as well as a number of other developmental decisions (25).

In this study, we test whether for certain fixed concentrations of total cyclin a frog egg extract can arrest stably in either interphase or mitosis; i.e., the Cdc2 control system is bistable. Bistability has been observed in the budding yeast cell cycle where, under identical culture conditions, a cell may arrest stably in either G_1 phase (low Cdk1 activity) or $S/G_2/M$ phase (high Cdk1 activity), depending on how the culture is prepared (26). In this study, we demonstrate bistability and hysteresis in frog egg extracts, suggesting that these dynamical properties of the Cdk control system may indeed be common regulatory features of eukaryotic cell cycles, as predicted (17, 20–23).

Methods

Cell-Free Egg Extracts. Cytostatic factor (CSF)-released and cycling egg extracts were prepared by the method of Murray (2). Extracts were released from CSF arrest with 0.4 mM $CaCl_2$. Unless otherwise indicated, extracts were supplemented with 500 sperm nuclei per μl. Cycling extracts were prepared by adding 5 μg/ml calcium ionophore A23187 (Sigma) to eggs before crushing. Where indicated, extracts were supplemented with 100 μg/ml cycloheximide (CHX) or 100 μg/ml aphidicolin (APH). At indicated times, 5 μl of extract was removed, fixed, and stained with 4′,6-diamidino-2-phenylindole fixative and observed by fluorescence and phase-contrast microscopy (2). Fields presented are representative of the entire slide. In some experiments, extract was removed at indicated times, diluted 10-fold in extraction buffer (27) containing 0.5 mM PMSF, 1 μM microcystin, and 3 μg/ml each leupeptin, pepstatin, and chymostatin, and snap-frozen for immunoblotting or H1 kinase assays.

Preparation of Nondegradable Cyclin B. Bacculovirus encoding histidine-tagged nondegradable human cyclin B (Δcyclin B) from William Dunphy (28) (Howard Hughes Medical Institute, California Institute of Technology, Pasadena) was used to infect SF9 cells. Cell pellets were lysed, and protein was purified on Ni-NTA agarose (Qiagen, Chatsworth, CA) and eluted with 200 mM imidizole. Purity was confirmed by Coomasie blue staining of protein resolved by SDS/PAGE. Total volume of Δcyclin B added to extracts was <8%.

Immunoblotting and Histone H1 Kinase Assays. Immunoblotting of endogenous cyclin B was performed as described (29). Proteins were resolved on 10% Laemmli acrylamide gels. Histone H1 kinase assays were performed as described (27).

Model Simulations. All calculations were done on the Novak–Tyson model (17) by using the parameter values estimated by Marlovits *et al.* (30), with two exceptions. (*i*) $[Cdc2]_{total} = 80$ nM in these simulations because Fig. 6*b* indicates that 80 nM cyclin B is sufficient to bind the entire pool of Cdc2. (*ii*) The values of k_w and k_{25} were reduced by 40% (to 1 min^{-1}), because our cyclin B preparation seems to be less active than that of Kumagai and Dunphy (28), on which previous estimates were based.

Results and Discussion

The Threshold Concentration of Cyclin to Enter Mitosis Is Higher than the Threshold Concentration of Cyclin to Exit Mitosis. The Novak–Tyson model predicts that the cyclin threshold to enter mitosis is higher than the threshold to exit mitosis (Fig. 1*a*). In this case, there exists a range of intermediate cyclin concentrations that will maintain a mitotic extract in mitosis but will not trigger entry into mitosis in an interphase extract.

To test the prediction of hysteresis, we measured threshold concentrations of cyclin, marking transitions into and out of M phase in the same egg extract preparation. Extracts were made dependent on fixed concentrations of exogenous Δcyclin B by supplementing them with CHX to prevent synthesis of endogenous proteins (28).

To measure the inactivation and activation thresholds during the same M phase, cycling extracts (2) that autonomously enter and exit mitosis I were prepared (Fig. 2 *a–c*). Eggs were first released from meiosis II with calcium ionophore, then crushed and processed into extracts. Sperm nuclei were added to extracts to monitor cell-cycle progression (mitosis = condensed chromatin, no nuclear envelope; interphase = decondensed chromatin, distinct nuclear envelope). By the time Δcyclin B was added ($t = 0$), the extracts were in first interphase. CHX was added at 0 min (interphase) for the activation threshold (Fig. 2*a*) or at 60 min (mitosis I) for the inactivation threshold (Fig. 2*b*). These data indicate that the activation threshold for mitosis I lies between 32 and 40 nM Δcyclin B (Fig. 2*a*) and the inactivation threshold lies between 16 and 24 nM Δcyclin B (Fig. 2*b*). Intermediate concentrations of 24 and 32 nM could support either interphase or mitosis, depending on starting conditions, confirming bistability and hysteresis.

This interpretation of the data assumes that mitotic cyclins are the only relevant proteins synthesized between interphase (when CHX was added for activation threshold measurements) and mitosis I (when CHX was added for inactivation threshold measurements). However, Cdc25A is synthesized during the first cell cycle in the intact embryo (31) and therefore, distinct activation and inactivation thresholds might result in part from differences in level of Cdc25A. However, in a modified protocol, the inactivation threshold was measured in cycling extracts treated with CHX and Δcyclin B at 0 min, using exogenous degradable cyclin B to drive the extract into mitosis and varying amounts of Δcyclin B to hold the extracts in mitosis. In this case, the inactivation threshold was also 2- to 3-fold smaller than the activation threshold even through protein synthesis was halted at the same time for both measurements (data not shown).

To verify that CHX inhibits synthesis of endogenous cyclins,

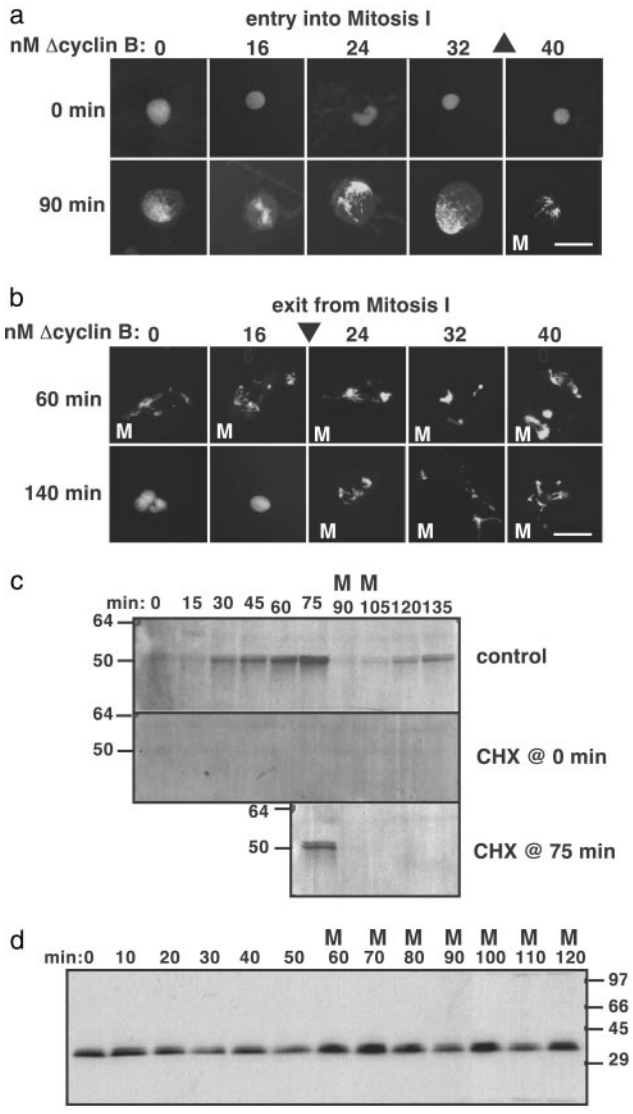

Fig. 2. The threshold concentration of cyclin B to enter mitosis is higher than the threshold to exit mitosis. Cycling egg extracts in interphase of cycle 1 were supplemented with Δcyclin B (at $t = 0$). (*a*) To measure the activation threshold, CHX was added immediately ($t = 0$). (*b*) To measure the inactivation threshold, CHX was added 60 min later when the extract was in mitosis. Fluorescence micrographs of sperm nuclei are depicted. Triangles denote activation threshold (▲) and inactivation threshold (▼) concentrations. (Scale bars = 50 μm.) (*c*) Extracts prepared as in *a* and *b* without exogenous cyclin were immunoblotted for endogenous cyclin B1. (*d*) A CHX-treated CSF-released extract was supplemented with 150 nM Δcyclin B during interphase ($t = 0$). Samples were collected and blotted for Δcyclin B. Extracts are labeled M when >90% nuclei on a slide appear mitotic (condensed chromatin, no nuclear envelope). In unlabeled extracts, >90% nuclei were in interphase. Migration of molecular mass standards (in kDa) is indicated.

the level of endogenous cyclin B1 (as a representative mitotic cyclin) was monitored in cycling extracts treated with CHX as in Fig. 2 *a* and *b* (Fig. 2*c*). Endogenous cyclin B1 is degraded rapidly at both meiosis II and mitosis I, and CHX added at 0 or 75 min prevents its reaccumulation. Similar results were obtained when blots were probed for cyclins A1 and B2 (not shown). Immunoblotting of exogenous Δcyclin B in egg extracts indicates that the protein remains stable in egg extracts (Fig. 2*d*).

The Amplitude of the Down Jump in Cdc2 Activity Is Less than That of the Up Jump. Measurement of distinct activation threshold and inactivation threshold concentrations of cyclin for entry into and exit from mitosis confirms the fundamental prediction of hysteresis underlying the mitotic cycles of cell-free egg extracts. The Novak–Tyson model makes additional, specific predictions regarding Cdc2 activity near these thresholds. (*i*) As cyclin concentration is increased toward the activation threshold, Cdc2 activity is very low and then jumps abruptly to high activity. This prediction agrees well with measurements made by Solomon *et al.* (4). (*ii*) On the other hand, as cyclin concentration is decreased toward the inactivation threshold, Cdc2 kinase activity drops lower and lower (because there is less and less cyclin available). Finally, at the inactivation threshold, Cdc2 activity drops to the very low value, but the amplitude of the down jump is much less dramatic than the up jump. To test this quantitative prediction experimentally, Cdc2 activity was measured by phosphorylation of histone H1 in cycling extracts prepared as in Fig. 2 *a–c* and compared with numerical simulations of the Novak–Tyson mathematical model (Fig. 3). Concentrations of cyclin were selected to bracket the inactivation threshold (≈16 nM). At 90 min, all CHX-treated extracts remained in interphase except those supplemented with 60 nM Δcyclin B (Fig. 3*a*). Correspondingly, H1 kinase activity was high in the M-phase extract and low in all others, as predicted. To fit these data to numerical simulations, H1-kinase activity (pmol ^{32}P incorporated) was correlated to theoretical Cdc2 activity (arbitrary units). We assume that $A \times M = P - B$, where P = H1-kinase activity, B = background activity, M = M-phase promoting factor (Cdc2)

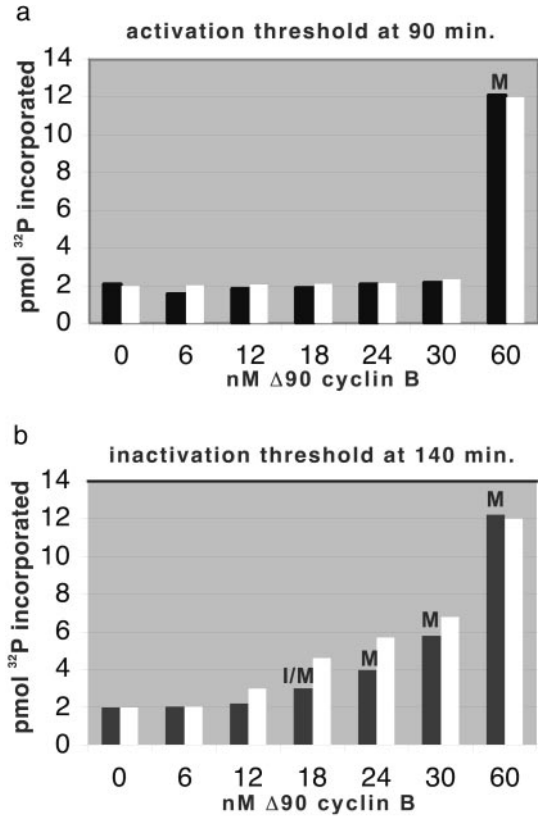

Fig. 3. The amplitude of the down jump in Cdc2 activity is less than that of the up jump. Samples from cycling extracts prepared as in Fig. 2 were analyzed for Cdc2 kinase activity as measured by incorporation of ^{32}P from [γ-^{32}P]ATP into histone H1. (*a*) Activation threshold as in Fig. 2*a*. (*b*) Inactivation threshold as in Fig. 2*b*. Experimental data (black bars) are compared with numerical simulations of the Novak–Tyson model (white bars). Extracts are labeled M when >90% nuclei on a slide appear mitotic (condensed chromatin, no nuclear envelope). In extract labeled I/M (*b*), 58% nuclei were in mitosis.

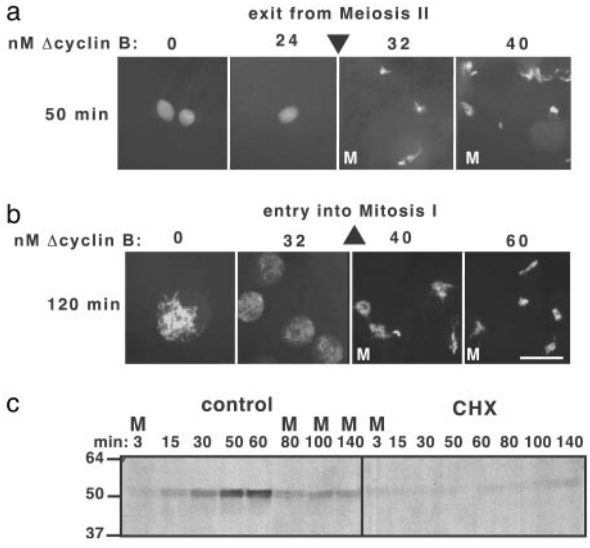

Fig. 4. The threshold concentration of cyclin B to enter mitosis I is higher than the threshold to exit meiosis II. (*a*) To measure the cyclin threshold for exit from meiosis II, CSF extract was supplemented with CHX and Δcyclin B, then released from CSF arrest by addition of calcium (at $t = 0$) and photographed under fluorescence microscopy at 50 min. (*b*) To measure the cyclin threshold for entry into mitosis I, Δcyclin B was added to CHX-treated CSF-released extract at 50 min (when extract was in interphase), and nuclei were photographed at 120 min. Thresholds in *a* and *b* were measured in the same extract preparation. Triangles denote threshold concentrations. (Scale bar = 50 μm.) (*c*) Extracts prepared as in *a* and *b*, without exogenous cyclin, were immunoblotted for endogenous cyclin B1.

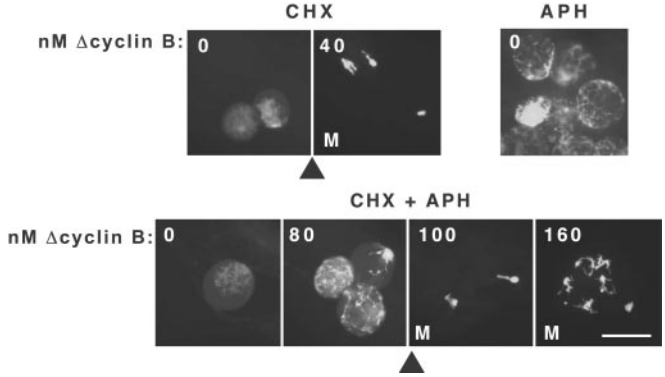

Fig. 5. The cyclin threshold for Cdc2 activation is raised by unreplicated DNA. CSF-released extracts containing 1,200 nuclei per μl were supplemented at 0 min with CHX, APH, or both (CHX + APH). ΔCyclin B was added at 40 min (interphase). Photographs of sperm nuclei were taken under fluorescence microscopy at 140 min. Extracts are labeled M when >90% nuclei on a slide appear mitotic. Triangle denotes threshold concentration of cyclin. (Scale bar = 50 μm.)

activity in model, A = scaling constant. Using the data in Fig. 3*a*, $A = 15$ and $B = 2$.

In extracts treated with CHX at 75 min (M phase) to measure the inactivation threshold concentration of cyclin B (Fig. 3*b*), Cdc2 activity was low in samples that exited mitosis by 140 min (0–12 nM Δcyclin B) and gradually higher in samples that remained in mitosis (24–60 nM Δcyclin B). Cdc2 activity was proportional to the concentration of Δcyclin B above the inactivation threshold (Fig. 3*b*, black bars), in agreement with Fig. 1*a* and numerical simulations (Fig. 3*b*, white bars). The quantitatively good fit of theory to experiment in Fig. 3*b* is a valid test of the model because none of the data in Fig. 3*b* was used to estimate the coefficients A and B.

The Threshold Concentration of Cyclin to Exit Meiosis II Is Lower than the Threshold Concentration of Cyclin to Enter Mitosis I. We also compared the cyclin threshold for exit from meiosis II and entry into mitosis I. To measure the cyclin threshold for exit from meiosis, egg extracts arrested in meiosis II by CSF were prepared (Fig. 4). The extracts were supplemented with CHX and with different concentrations of Δcyclin B. At $t = 0$, the extracts were released from CSF arrest by addition of calcium. Extracts lacking Δcyclin B exited meiosis II within 15 min (not shown). The highest concentration of Δcyclin B that could still permit exit from meiosis II (the inactivation threshold) was 24 nM (Fig. 4*a*). Above this concentration, extracts remained stably in M phase for >70 min. In the same extract preparation, the activation threshold to enter mitosis I was determined by addition of Δcyclin B to the extract after it reached interphase (50 min) (Fig. 4*b*). Extracts lacking CHX entered mitosis at 80 min (not shown). By 120 min, only extracts supplemented with ≥40 nM Δcyclin B entered mitosis. Extracts supplemented with an intermediate concentration of 32 nM Δcyclin B remained in M phase if the protein was added during meiosis, and in interphase if the protein was added during interphase (Fig. 2 *a* and *b*). Hence, the cyclin threshold for entering mitosis I is higher than the cyclin threshold to exiting meiosis II. The difference between the thresholds was more subtle than was measured for entry into and exit from mitosis I in cycling extracts, but was highly reproducible. Activation thresholds were the same (40 nM) in Figs. 2*a* and 4*b*, whereas the inactivation threshold for exit from meiosis II was higher (24 nM < inactivation threshold < 32 nM; Fig. 4*a*) than for exit from mitosis I (16 nM < inactivation threshold < 24 nM; Fig. 2*b*). The different values may reflect fundamental differences between meiosis and mitosis or between CSF-released and cycling egg extracts.

Unreplicated DNA Raises the Threshold Concentration of Cyclin Required to Enter Mitosis. If hysteresis results from positive feedback regulating inhibitory phosphorylation of Cdc2, then conditions that oppose the positive feedback effect should raise the threshold concentration of cyclin required to drive entry into mitosis (17, 30). High concentrations of unreplicated DNA block cell-cycle progression (32) in egg extracts. The Novak–Tyson model (17) predicts that unreplicated DNA acts by raising the cyclin threshold, and hence a high level of cyclin may override the block to mitosis induced by unreplicated DNA.

To test this prediction, CSF-released extracts were supplemented with 1,200 sperm nuclei per μl and activated with calcium in the presence or absence of CHX and APH, an inhibitor of DNA polymerase (Fig. 5). ΔCyclin B was added to these extracts at 40 min (interphase). The APH-treated extract remained in interphase for the duration of the experiment (140 min) even in the absence of CHX (Fig. 5). As in Figs. 2*a* and 4*b*, the activation threshold was 40 nM in CHX-treated extracts without APH. In the presence of APH, the activation threshold was elevated to 80 nM < activation threshold < 100 nM Δcyclin B, confirming the predicted effect of unreplicated DNA on the hysteresis loop.

Although the fundamental effect of unreplicated DNA on the hysteresis loop validates the Novak–Tyson prediction, the proposed mechanism should be reconsidered in light of current data. Novak and Tyson hypothesized that a DNA replication checkpoint functioned by activating the phosphatase that catalyzes the dephosphorylation of Cdc25 and Wee1. It is now known that unreplicated DNA triggers a signaling network in which the kinase XChk1 positively regulates Wee1 (33) and negatively regulates Cdc25 (34). Phosphorylation increases the total amount of Wee1 in the nucleus and decreases the total amount of Cdc25 in the nucleus. Model calculations show that if

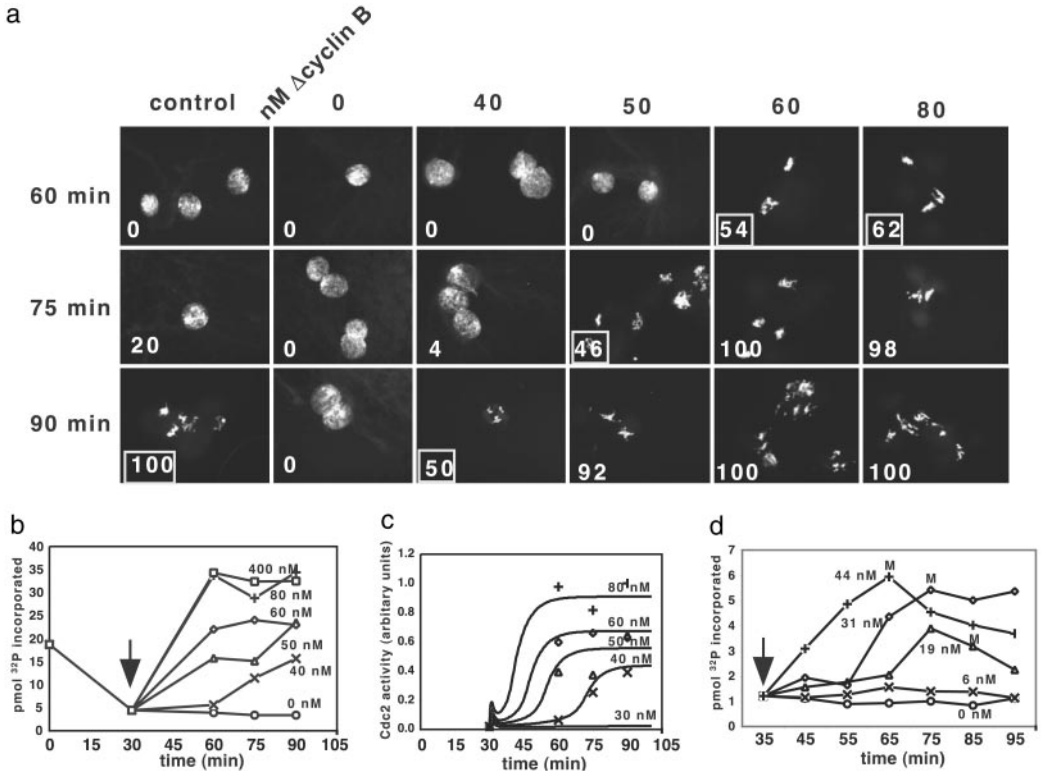

Fig. 6. Cdc2 activation exhibits a critical slowing down near the activation threshold concentration of cyclin B. CSF-released extracts were supplemented with CHX at 0 min and Δcyclin B at 30 min (interphase). Control extract lacking CHX entered mitosis at 90 min. Samples were collected every 15 min for microscopic analysis of nuclear morphology (*a*) and histone H1 kinase activity (*b*). In *a*, at each time is indicated the percent of nuclei (of 50 scored) that had undergone nuclear envelope breakdown and chromatin condensation. The extract was qualitatively scored as entering mitosis (boxed numbers) when >40% of the nuclei had condensed chromatin and no nuclear envelope. (*c*) Experimental data (symbols) from *b* are displayed alongside simulations of the Novak–Tyson model (curves). (*d*) Histone H1 kinase activity measured in an extract collected every 10 min with varying concentrations of Δcyclin B added at 35 min. M = time when nuclear morphology first indicated mitosis. Arrows denote addition of Δcyclin B in *b* and *d*. The preparation of Δcyclin B used in *d* was more active than the others, resulting in a lower activation threshold.

$[Wee1]_{total}$ increases 2-fold and $[Cdc25]_{total}$ decreases 2-fold, then the cyclin threshold for Cdc2 activation increases from 40 to 90 nM, in accordance with our observations. A mathematical model of the G_2 DNA damage checkpoint simulates the behavior of the XChk1 signaling pathway (35).

The Rate of Cdc2 Activation Slows Down Considerably Near the Activation Threshold Concentration of Cyclin. In the experiments shown in Figs. 2–5, the activation threshold was bounded between the highest concentration of Δcyclin B that would not drive nuclei into mitosis during the course of the experiment and the lowest concentration that would eventually drive >90% of nuclei into mitosis. For concentrations above threshold, Solomon *et al.* (4) and Clarke *et al.* (36) identified a lag time of 10–20 min (at 23°C) between addition of cyclin and activation of Cdc2 in CHX-treated extracts. The lag time was reported to be independent of the concentration of cyclin. However, the Novak–Tyson model predicts that lag time should correlate inversely with cyclin level at concentrations marginally above the activation threshold (17).

To resolve this discrepancy, CSF-arrested extracts were released by calcium at $t = 0$ and supplemented with CHX at 0 min and Δcyclin B at 30 min (interphase). Every 15 min, samples were collected to monitor sperm morphology (Fig. 6*a*) and assay for Cdc2 kinase activity (Fig. 6*b*). Nuclear morphology indicated that with 40 nM Δcyclin B, just above the activation threshold, the extract entered mitosis at 90 min, 60 min after the addition of Δcyclin B. At 50 nM, the lag time was 45 min. At 60 nM and above, the lag time was 30 min.

Cdc2 activity was also measured in the same extract (Fig. 6*b*) and compared with numerical simulations of the mathematical model (Fig. 6*c*). The fit between kinase activity and numerical simulation was good. However, by the time the first discriminative samples were collected at 60 min (30 min after addition of Δcyclin B, when mitosis was first observed in extracts containing 60 nM and above Δcyclin B), a jump in Cdc2 activity had already occurred in most of the samples. Therefore, a longer lag time for Cdc2 activation was observed only in the sample containing 40 nM cyclin B. To better observe the time window when Cdc2 was first activated at varying concentrations of Δcyclin B, the experiment was repeated and samples were collected for Cdc2 activity every 10 min after addition of Δcyclin B (Fig. 6*d*). In this study, distinct lag times for Cdc2 activation were measured for 19 nM (40-min lag), 31 nM (30-min lag), and 44 nM (10- to 20-min lag) Δcyclin B. The jump in Cdc2 activity preceded changes in nuclear morphology (M) by 10 or more min, explaining why some of the different lag times observed in Fig. 6*a* were missed in Fig. 6*b*.

Clearly, there is a distinct slowing down of the Cdc2 activation process as the cyclin threshold is approached from above, as predicted. An appreciable lag time is seen only for cyclin concentrations within 20 nM above threshold, which explains why the effect was not noticed by Solomon *et al.* (4).

Slowing down is a general property of dynamical systems close to saddle-node bifurcation points (the turning points at T_i and T_a in Fig. 1*a*). Hence, slowing down is another signature of the hysteresis loop that underlies transitions into and out of mitosis. Fig. 6 provides evidence for slowing down near the activation

threshold. Slowing down near the inactivation threshold is also predicted.

Conclusions

Bistability and hysteresis are new ways of looking at cell cycle control. Since the discovery of cyclins, their synthesis and degradation were predicted to be necessary for entry into and exit from mitosis (37), predictions that were elegantly confirmed in several studies (1, 14). But what causes cyclin degradation to turn on and off periodically as cells traverse the cell cycle? Why is it not the case for cyclins, as it is for most other proteins, that rates of synthesis and degradation balance each other throughout the cell cycle? There must be some mechanism for switching irreversibly between phases of net cyclin synthesis and net cyclin degradation. Novak and Tyson (17) proposed that a bistable switch is created by the positive feedback loops involving Cdc2, Wee1, and Cdc25 and that the irreversibility of cell cycle transitions is based on traverse around a hysteresis loop. These predictions and others are confirmed in this article.

J.M.'s contribution was performed mainly in the laboratory of Dr. Sally Kornbluth (Duke University Medical Center, Durham, NC). Her support is appreciated. We thank Felicia Etzkorn and Todd Stukenberg for their critiques and Bobby Johnson, Matthew Petrus, and Dayna Wilhelm for expert technical assistance. Antibodies were provided by Dr. James Maller (Howard Hughes Medical Institute, University of Colorado Health Sciences Center, Denver) and Dr. Julian Gannon (Cancer Research UK London Research Institute, Clare Hall Labs). This research was supported by grants from the National Institutes of Health–National Institute of General Medical Sciences (to J.C.S. and J.J.T.), Defense Advanced Research Project Agency–BioSPICE (to J.J.T.), the Carilion Biomedical Institute (to J.C.S.), and the Research Division of Virginia Polytechnic Institute.

1. Murray, A. W. & Kirschner, M. W. (1989) *Nature* **339,** 275–280.
2. Murray, A. W. (1991) *Methods Cell Biol.* **36**, 581–605.
3. Gautier, J., Minshull, J., Lohka, M., Glotzer, M., Hunt, T. & Maller, J. (1990) *Cell* **1990,** 487–494.
4. Solomon, M. J., Glotzer, M., Lee, T. H., Phillippe, M. & Kirschner, M. W. (1990) *Cell* **63,** 1013–1024.
5. Mueller, P. R., Coleman, T. R. & Dunphy, W. G. (1995) *Mol. Biol. Cell* **6,** 119–134.
6. Mueller, P. R., Coleman, T. R., Kumagai, A. & Dunphy, W. G. (1995) *Science* **270,** 86–90.
7. Gautier, J., Solomon, M. J., Booher, R. N., Bazan, J. F. & Kirschner, M. W. (1991) *Cell* **67,** 197–211.
8. Kumagai, A. & Dunphy, W. G. (1991) *Cell* **64,** 903–914.
9. Smythe, C. & Newport, J. W. (1992) *Cell* **68,** 787–797.
10. Kumagai, A. & Dunphy, W. G. (1992) *Cell* **70,** 139–151.
11. Izumi, T. & Maller, J. L. (1993) *Mol. Biol. Cell* **4,** 1337–1350.
12. Felix, M. A., Labbe, J. C., Doree, M., Hunt, T. & Karsenti, E. (1990) *Nature* **346,** 379–382.
13. Lorca, T., Castro, A., Martinez, A. M., Vigneron, S., Morin, N., Sigrist, S., Lehner, C., Doree, M. & Labbe, J. C. (1998) *EMBO J.* **17,** 3565–3575.
14. Murray, A. W., Solomon, M. J. & Kirschner, M. W. (1989) *Nature* **339,** 280–286.
15. Holloway, S., Glotzer, M., King, R. W. & Murray, A. W. (1993) *Cell* **73,** 1393–1402.
16. Stemmann, O., Zou, H., Gerber, S. A., Gygi, S. P. & Kirschner, M. W. (2001) *Cell* **107,** 715–726.
17. Novak, B. & Tyson, J. J. (1993) *J. Cell Sci.* **106,** 1153–1168.
18. Tyson, J. J. & Novak, B. (2001) *J. Theor. Biol.* **210,** 249–263.
19. Goldbeter, A. (1991) *Proc. Natl. Acad. Sci. USA* **88,** 9107–9111.
20. Tyson, J. J. (1991) *Proc. Natl. Acad. Sci. USA* **88,** 7328–7332.
21. Nasmyth, K. (1996) *Trends Genet.* **12,** 405–412.
22. Thron, C. (1997) *Oncogene* **15,** 317–325.
23. Tyson, J. J., Novak, B., Odell, G. M., Chen, K. & Thron, C. D. (1996) *Trends Biochem. Sci.* **21,** 89–96.
24. Ferrell, J. E., Jr., & Machleder, E. M. (1998) *Science* **280,** 895–898.
25. Ferrell, J. E., Jr., & Xiong, W. (2001) *Chaos* **11,** 227–236.
26. Cross, F. R., Archambault, V., Miller, M. & Klovstad, M. (2002) *Mol. Biol. Cell* **13,** 52–70.
27. Kappas, N., Savage, P., Chen, K. C., Walls, A. T. & Sible, J. C. (2000) *Mol. Biol. Cell* **11,** 3101–3108.
28. Kumagai, A. & Dunphy, W. G. (1995) *Mol. Biol. Cell* **6,** 199–213.
29. Hartley, R. S., Sible, J. C., Lewellyn, A. L. & Maller, J. L. (1997) *Dev. Biol.* **188,** 312–321.
30. Marlovits, G. (1998) *Biophys. Chem.* **72,** 169–184.
31. Kim, S., Li, C. & Maller, J. (1999) *Dev. Biol.* **212,** 381–391.
32. Dasso, M. & Newport, J. W. (1990) *Cell* **61,** 811–823.
33. Lee, J., Kumagai, A. & Dunphy, W. G. (2001) *Mol. Biol. Cell* **12,** 551–563.
34. Kumagai, A., Guo, Z., Emami, K. H., Wang, S. X. & Dunphy, W. G. (1998) *J. Cell Biol.* **142,** 1559–1569.
35. Aguda, B. (1999) *Proc. Natl. Acad. Sci. USA* **96,** 11352–11357.
36. Clarke, P. R., Leiss, D., Pagano, M. & Karsenti, E. (1992) *EMBO J.* **11,** 1751–1761.
37. Evans, T., Rosenthal, E. T., Youngblom, J., Distel, D. & Hunt, T. (1983) *Cell* **33,** 389–396.